Quantum Efficiency of Cold Electron Bolometer Optical Response

Mikhail A. Tarasov, Valerian S. Edelman, Andrey B. Ermakov, Sumedh Mahashabde, and Leonid S. Kuzmin

Abstract—In this paper, we present the measurements of optical response dependence on power load of a Cold Electron Bolometer integrated in a twin slot antenna. These measurements are also compared to the models of the bolometer limit and the photon counter limit. The responsivity of $0.22 * 10^9$ V/W was measured at 0.22 pW radiation power from a black body at 3.5 K. According to our estimations, for optimized device the voltage responsivity at 100 mK electron temperature can approach $S_v = 10^{10}$ V/W for power load below 0.1 pW and decreases down to 10^7 V/W at 300 mK for 5 pW signal power in a sample with absorber volume of $5 * 10^{-20}$ m^3. In the case of low bath temperatures and high applied RF power the changes of tunneling current, dynamic resistance and voltage response are explained by non-thermal energy distribution of excited electrons. Distribution of excited electrons in such system at lower temperatures can be of non-Fermi type, hot electrons with energies of the order of 1 K tunnel from normal metal absorber to superconductor instead of relaxing down to thermal energy kT_e in absorber before tunneling. This effect can reduce quantum efficiency of the bolometer at 350 GHz from $\eta = hf/kT_{\rm ph} > 100$ in ideal case down to single electron per absorbed photon ($\eta = 1$) in the high power case. Methods of preserving high quantum efficiency are discussed.

Index Terms—Bolometers, nanofabrication, slot antennas, sub-millimeter-wave technology, superconducting devices.

I. INTRODUCTION

C OLD ELECTRON bolometer, with superconductor–insulator–normal metal–insulator–superconductor (SINIS) structure, has promising predicted performance [1], [2]. Under microwave irradiation the electron temperature of the absorber increases above the phonon temperature. Excited electrons with energy higher than the Fermi level in the normal metal volume can cause an increase in the tunneling current and/or decrease of

dc voltage across the bolometer and this response is dependent on applied power and frequency. Theoretical estimations usually assume that heating due to microwave radiation is equivalent to the dc heating at the same absorbed power. However in a normal metal, for radiation at Terahertz frequencies ($f \gg kT_e/h$) the process of absorption of photons by single electrons with energy $E = hf \gg kT_e$ dominates [3]–[6]. In this case the energy distribution of electrons is determined by a balance of processes of photon quantum absorption, electron–electron interactions, electron–phonon interactions, phonon–electron interactions, phonon escape, and tunneling of excited electrons in a SIN junction [3], [4]. This resulting distribution is significantly different from equilibrium Fermi distribution. Calculations of tunneling current using the microscopic theory in the clean limit [3], [4] for electron–electron and electron–phonon collision integrals show that increase of current response is dependent on multiplication of excited electrons with energies $E > kT_e$ due to electron–electron interactions and reabsorption of nonequilibrium phonons that do not escape from absorber. Multiplication of excited electrons leads to increase of current response $\delta I(P)$, where P is the absorbed power, and to an increase in current δI in the voltage bias mode. Thus current response δI of SINIS detector can exceed the photon counter limit of $dq/dE = e/hf$, and in some cases approaching the bolometric response limit of e/kT_e. Studies and optimization of energy relaxation in electron system at low temperatures can help to improve the optical response of practical SINIS detectors.

In our earlier experiments [7], [8], [15] we observed voltage response $\delta V(I) = V_{I,P=0} - V_{I,P}$, which indicates a nonequilibrium distribution in electron system. Here we have performed detailed analysis of new experimental data on I–V curves, dynamic resistance, optical response to show absence of equilibrium in electron system and significant tunneling current due to electrons with excess energy.

II. BOLOMETER AND RADIATION SOURCE

Bolometers containing 3 serial SINIS structures were integrated in a twin-slot antenna. The normal metal in the SINIS structure was a 10 nm thick layer of Aluminum whose superconductivity was suppressed by a thin (0.5 nm) layer of Iron (Fe) [9]. The geometry is shown in Fig. 1. For matching the impedance of the bolometers to the antenna, they were connected in parallel by means of a thin film capacitor as shown in Fig. 2. For measurement of dc response, they were connected in series due the insulation offered by the capacitor. Dimensions of elements are the following: area of tunnel junctions $-0.25\,\mu{\rm m}^2$,
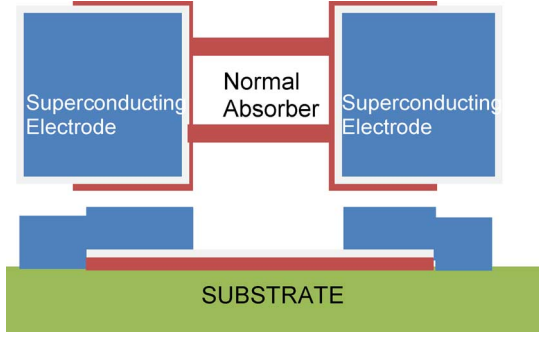
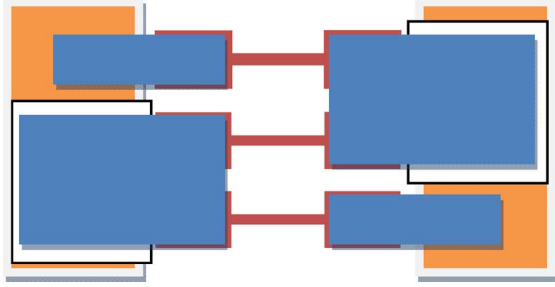Fig. 1.   Schematic view of SINIS, in-plane (top), cross-section (bottom).

Fig. 2.   The schematic view of three bolometers connected in series for DC and in parallel for microwave signal. White boxes represent insulator between electrodes (orange) and connecting Al top electrode (blue).

length, width, and thickness of normal metal absorber $-1*0.1*0.01\ \mu m^3$, dc resistance of single absorber—ca.200 Ω.

Parallel connection of detectors for microwave signal creates a load impedance of 60 Ω at the antenna terminal. Tunnel junction parameters were similar to those reported in [7], [8]. When cooling down to T $<$ 0.1 K the resistance ratio $R_{d(V=0)}/R_n$ (where $R_d = dV/dI$, R_n – asymptotic normal resistance) approached $R_d/R_n = 15000$, and total resistance of array at 0.1 K approached $R_{d(V=0)} = 400$ MΩ. This dynamic resistance should not be confused with load impedance at the antenna terminals. The capacitance of the NIS tunnel junctions effectively shunts this dynamic resistance in the microwave frequency range.

The samples were measured in a dilution cryostat equipped with a pulse tube refrigerator [10]. An additional recondensing stage with liquefying of Helium gas in a 0.12 L container allows the operating temperature to be maintained below 0.1 K for a period of 4–5 h with compressor shut down. Sample with SINIS receiver was mounted on the dilution chamber inside a copper radiation shield at temperature 0.4 K, the inner wall of which was painted with black absorbing paint containing Stycast® 2850 FT.

The sample fabricated on a silicon substrate 0.35 mm thick was attached to a sapphire hyperhemispheric lens of 10 mm in diameter that coupled radiation to the planar antenna. Lens itself was glued with Stycast® 1266 in a copper holder screwed to the dilution chamber. Separate measurements with RuO$_2$ thermometer glued to a Si plate instead of detector show that its temperature at 0.1 K differs by less than 2–3 mK from mixing

chamber temperature measured by LakeShore® thermometer with absolute error below 5 mK.

An aperture of 5 mm in diameter was created in front of the lens at the bottom of radiation shield to attach two planar bandpass filters [11] for central frequency of 330 GHz and total bandwidth of 50 GHz. Spectral transmission of these filters can be described within 10% accuracy by product of two Lorentz lines with FWHM of 70 GHz. Maximum transmission in the pass-band was over 90%. Distance from the lens to filters is 2–3 mm, between filters 2 mm, and from filter to the black body source 2–3 mm.

Radiation source is a black body made on Si wafer covered with NiCr film of square resistance of 300 Ω. This wafer was mounted on copper plate with thermally insulated legs on the 1 K pot. Temperature of radiation source was monitored by measuring resistance of a calibrated RuO$_2$ chip-resistor and heating power was varied by current through this NiCr film in the range of 2–15 K. Dissipated power was up to few milliwatts, time constant for heating/cooling of the order of 0.1 s.

Power received by antenna was calculated using Planck formula for single mode

$$P_{\text{incident}} = \int df \frac{hf}{\exp(\frac{hf}{kT_R}) - 1} * K1 * K2 * K3 \quad (1)$$

where T_R is the radiation source temperature, factors $K1$ and $K2$ account for transmission of filters and spectral matching to the antenna. For twin-slot antenna we assume a Lorentzian function of the line shape with a half-width of 100 GHz and maximum at 330 GHz. Influence of $K2$ brings reducing of incident power by about 0.8. Multiplier $K3 = 0.72$ takes into account reflections at the sapphire–silicon and sapphire–vacuum interfaces.

III. EXPERIMENTAL I-V CURVES AND ESTIMATIONS OF EQUIVALENT ELECTRON TEMPERATURE

A. Response to Bath Temperature

Equivalent electron temperature in a normal metal absorber was deduced from dependence of measured dynamic resistance $R_d = dV/dI$ and comparison with dV/dT_e dependence of an ideal SIN junction at some effective electron temperature. The I–V curve of ideal SIN junction for single junction can be presented as [1]

$$I = \frac{1}{eR_N} \int_{-\infty}^{\infty} \nu(E)(f_N(E - eV) - f_S(E))\,dE. \quad (2)$$

In Fig. 3(a), (b) we present IV curves for two electron temperatures and calculation according to (2). In our case we have 6 junctions connected in series, so measured values of R_n and V are divided by 6 to compare with the modeled curve. In experimental curves the measured voltage corresponds to $6*V_{\text{SIN}}$ where V_{SIN} is the voltage across the single SIN junction.

The superconducting gap voltage V_Δ can be expressed as $eV_\Delta = \Delta(0) = 1.76*kT_c$, according to the BCS theory where T_c is the critical temperature of the superconductor. It can be
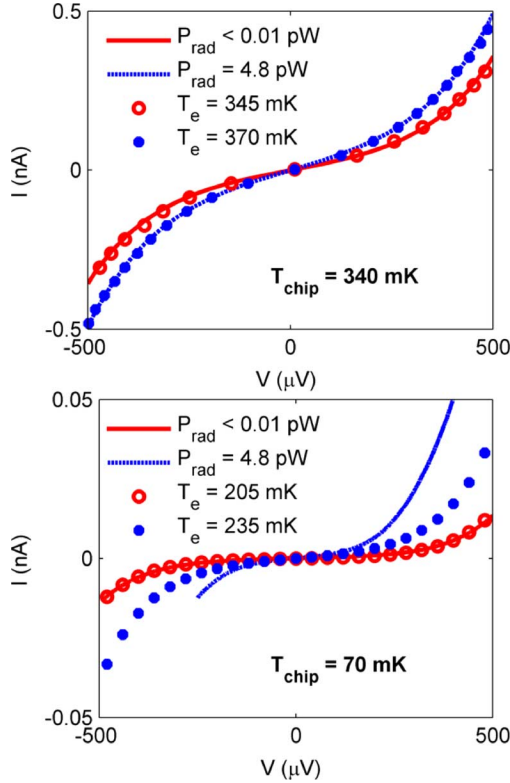
Fig. 3. (Upper) IV curves of SINIS bolometer at bath temperature 340 mK and (Lower) 70 mK. Solid lines correspond to experimental data obtained at two radiation power levels of 4.8 pW and below 10 fW. Stars and circles – calculated curves for 345 mK and 370 mK (upper), and 205 mK and 235 mK (lower).

determined from the dependence $R_{d(T,V=0)}$ on bath temperature, which has exponential dependence in the bath temperature range of 0.3 K to 0.5 K. At higher temperatures the temperature dependence of the superconducting gap $\Delta(T)$ should also be accounted for. At temperatures below 0.2 K the dynamic resistance R_d approaches a constant value that can be explained by overheating of electron system by external radiation. The value of equivalent T_e can be estimated by fitting experimental data with (2). In our fitting we use value of Δ that corresponds to $T_c \sim 1.4$ K and using $\Delta = k * 2.45$ K we obtained good correspondence of experimental curves to the model. Small difference can be observed at $V > 0.4$ mV where resistance is higher compared to calculated one due to the effect of electron cooling.

B. Response to Microwave Radiation

If the electron system of absorber is heated up by absorbed radiation, then the I–V curve is different from the case of increase of the bath temperature, see Fig. 3 (lower). There is no more correspondence with a simple thermal model. If we assume T_e for which $R_{d(V=0)}$ is the same as in model, then at higher bias current the difference in resistance can be more than 10 times larger. One can see that power response and temperature response are different at 70 mK and coincide at 340 mK (Fig. 4).

Dependence of responsivity dV/dP on bath (phonon) temperature and on equivalent electron temperature are presented in Fig. 5 (upper, lower) for radiation power levels of 0.22, 1.36,
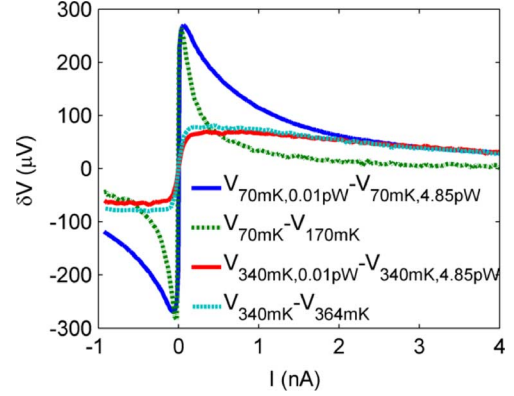

Fig. 4. Voltage response dependence on dc bias current for bath temperatures of 70 mK and 340 mK. Solid lines measured under 4.85 pW radiation power, dashed – response to equivalent increase in temperature without irradiation.

2.93, and 4.85 pW. When plotted in dependence on electron temperature (Fig. 5, lower), the shape of dV/dP curve shows that the responsivity is actually dependent on nonequilibrium electron temperature. The dependence of responsivity on electron temperature is proportional to T^{-4}, as is predicted in theory [1]. When irradiated with ca. 5 pW power the responsivity is reduced by an order of magnitude compared to 0.01 pW power load case. When bath is heated to 0.34 K these responsivities become equal for all power loads meaning that in this temperature range the detector becomes linear, dV/dP is independent on power and responsivity is determined by bath temperature. In this case electron and phonon temperatures are very close, and nearly equal. It means that increase of bath temperature leads to increase of relaxation processes and thermalization of electron system.

Losses in the bolometer can be roughly estimated from power to current transfer ratio, or current responsivity. We can compare a number of incoming quanta $I_Q = 5 * 10^8$ s^{-1} for 0.1 pW at frequency 330 GHz and a number of excited electrons that tunnel due to irradiation $I_S = 6 * 10^8$ s^{-1} (current increase at this power load). Quantum efficiency $\eta = I_S/I_Q = 1.2$ is close to unity, which means that one quantum produces just one electron, that is a photon counter mode. There is no multiplication of excited electrons number which was expected in [4] for bolometric mode of operation. If energy does not escape from the electron system, then the number of excited electrons with energies in the range of 0.2Δ to 1Δ should be $hf/kT = 30$ times more.

IV. DISCUSSION

According to estimations from [12] the difference of calculated and experimental curves proves the absence of equilibrium in electron system when energy distribution for electrons with energy above the Fermi level and holes with energy below the Fermi level does not correspond to Fermi distribution with equivalent electron temperature. These excited electrons can be treated in two groups: thermalized and athermal. Impact of thermalized electrons can be estimated assuming that their temperature corresponds to the calculated one for the case when calculated curve is a tangent to the experimental curve at $V = 0$, and dynamic resistances in both cases are equal. In Fig. 3(lower)
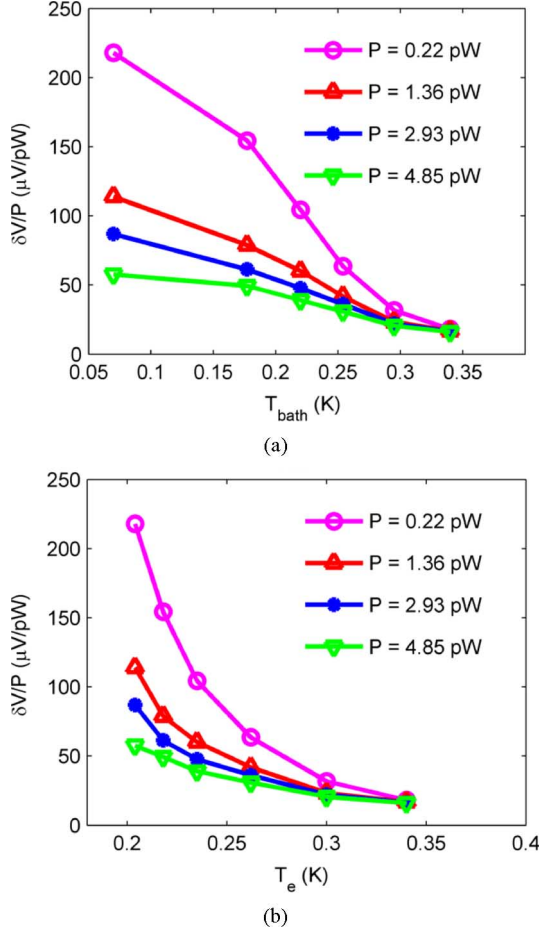
(a)

(b)

Fig. 5. Responsivity dependence on (a) bath temperature and on (b) equivalent electron temperature for radiation power levels of 0.22, 1.36, 2.93, 4.85 pW at black body temperatures 3.5, 6, 8.5, and 11 K.

Fig. 6. Dependencies of time constants τ_{diff}, τ_{sin}, τ_{escape}, τ_{ep}, τ_{pe}, τ_{ee}, and τ_{pp} on excitation energy plotted in Kelvins i.e., E/k.

such assumption leads to the electron temperature estimation of 235 mK under irradiation. The impact from athermal electrons can be estimated as a difference between measured and calculated current and can be up to 70% of the total response. When temperature increase the relaxation processes speed-up and at 340 mK the impact from athermal electrons is much lower. At the same time the impact from thermalized electrons increase, they prevail in tunneling current. As a result the dc bias voltage dependence of voltage to power response approaches the calculated one.

Radiation power is coupled to a normal metal absorber with dimensions much less as compared to the wavelength, so it can be considered as a lumped element. When absorbing the single quantum of radiation energy of $hf/k = 16$ K, all this energy is transferred to an electron, it forms electron-hole pair with energies from 0 to hf above/below the Fermi energy. The average energy of excited electron and hole is 8 K.

Excited electrons and holes diffuse towards the area of tunnel junctions with diffusion time τ_{diff}, then transfer into superconducting electrode with time constant τ_{SIN}. During this time period the energy is redistributed due to electron–phonon, phonon–electron, electron–electron, phonon–phonon and phonon escape processes. As a result energy of excited electrons is reduced, their number can increase, some power escape
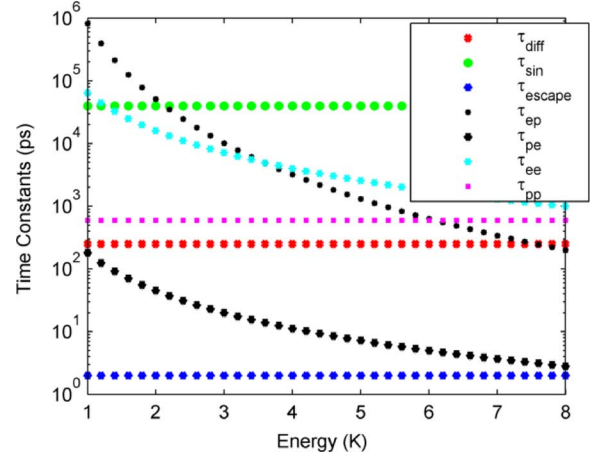
into substrate and superconducting electrodes. Additional tunneling current under irradiation depends on ratio of time constants of these processes. Since all the time constants are strongly dependent on excitation energy, the dynamics become very complicated, especially taking into account transition from two-dimensional to three-dimensional cases when changing temperature and power. Overheating processes in superconducting electrode are usually ignored in rough estimations; superconductor is assumed as a thermal sink. From the above considerations and taking into account a microscopic model described in [13], [14] it is clear that due to complicated combination of electron–electron, electron–phonon, phonon–electron interactions which vary with signal frequency and power, the energy distribution of electrons is much different from simple Fermi distribution. Nonequillibrium of system is mainly determined by ratio of escape time for electrons due to tunneling τ_{sin} to electron-electron and electron–phonon time constants. Finally, we can pick out two groups of time constants, the first is energy independent like diffusion time $\tau_{\text{diff}} = 0.25$ ns, tunneling time $\tau_{\text{sin}} = 40$ ns, phonon escape time $\tau_{\text{escape}} = 2$ ps, and phonon-phonon time $\tau_{\text{pp}} = 0.6$ ns. Energy dependent time constants are second-order dependent $1/E^2$ electron–electron time τ_{ee} and τ_{pe}, and also a fourth-order dependent $1/E^4$ electron–phonon constant τ_{ep}. The dependence of these time constants on energy is presented in Fig. 6.

Electron-electron and electron–phonon time constants become equal at energy around 3.7 K, and for lower energies electron–phonon interaction get slower, so electron–electron interaction can become dominating. To increase bolometer efficiency the length of absorber should be increased providing diffusion time τ_{diff} longer as compared to τ_{ee} and τ_{ep}. The value of τ_{ep} should be increased by using absorber material with lower electron–phonon parameter Σ. The resistivity, density, and acoustic impedance of absorber material should be increased as well. According to [3] the optimal resistance of SIN junction should be around 10 kΩ.

V. CONCLUSION

Nonequilibrium in electron system plays a critical role in optical response and performance of SINIS detectors. Highest re-

sponsivity can be achieved for maximum multiplication of electrons in absorber due to electron-electron interactions and absorption of nonequilibrium phonons. Time of electron–electron collisions exceeds electron–phonon time at the beginning of relaxation process and this diminishes multiplication. Nonequilibrium of phonon system is determined by phonons escaping to superconducting electrode that is fabricated from the same aluminum as absorber. The natural way to increase multiplication of excited electrons and increase response of detector is using material with lower τ_{ee}, higher τ_{ep}, and higher acoustic mismatch with aluminum – an interesting candidate being Hafnium. Inversion of sequence of layers with placing absorber above superconductor can also reduce the phonon escape to substrate. An important improvement in present work is increasing of superconducting electrode thickness that reduces overheating of superconductor and in turns reduces the overheating of absorber by back tunneling electrons.

The estimated responsivity decreasing from 10^{10} V/W at 100 mK down to 10^8 V/W at 300 mK corresponds to increasing of NEP from 10^{-18} W/Hz$^{1/2}$ up to 10^{-16} W/Hz$^{1/2}$ for the noise level of 10^{-8} V/Hz$^{1/2}$ determined by the readout amplifier noise.

REFERENCES

[1] L. Kuzmin, "On the concept of a hot-electron microbolometer with capacitive coupling to the antenna," *Phys. B: Condens. Mater.*, vol. 284–288, p. 2129, 2000.

[2] L. Kuzmin, "Array of cold-electron bolometers with SIN tunnel junctions for cosmology experiments," in *J. Phys.: Conf. Series*, 2008, vol. 97, p. 012310.

[3] I. Devyatov and M. Kupriyanov, "Investigation of a nonequilibrium electron subsystem in low-temperature microwave detectors," *JETP Lett.*, vol. 80, no. 10, pp. 646–650, 2004.

[4] I. Devyatov, P. Krutitsky, and M. Kupriyanov, "Investigation of various operation modes of a miniature superconducting detector of microwave radiation," *JETPh Lett.*, vol. 84, no. 2, pp. 57–61, 2006.

[5] A. Semenov, I. Devyatov, and M. Kupriyanov, "Theoretical analysis of the operation of the kinetic-inductance based superconducting microwave detector," *JETP Lett.*, vol. 88, no. 7, pp. 514–520, 2008.

[6] P. Virtanen, T. T. Hekkila, F. S. Bergeret, and J. C. Cuevas, "Theory of microwave-assisted supercurrent in diffusive SNS junctions," *Phys. Rev. Lett.*, vol. 104, p. 247003, 2010.

[7] M. Tarasov, L. Kuzmin, V. Edelman, N. Kaurova, M. Fominsky, and A. Ermakov, "Optical response of a cold-electron bolometer array," *JETP Lett.*, vol. 92, no. 6, pp. 416–420, 2010.

[8] M. Tarasov, V. Edelman, L. Kuzmin, P. de Bernardis, and S. Mahashabde, "Optical response of a cold-electron bolometer array integrated in a 345 GHz cross-slot antenna," *IEEE Trans. Appl. Supercond.*, vol. 21, no. 6, p. 3635, 2011.

[9] M. A. Tarasov, L. S. Kuz'min, and N. S. Kaurova, "Thin multilayer aluminum structures for superconducting devices," *Instr. and Exp. Techn.*, vol. 52, no. 6, pp. 877–881, 2009.

[10] V. Edelman and G. Yakopov, "A dilution microcryostat cooled by a refrigerator with an impulse tube," *Instr. and Exp. Techn.*, vol. 56, no. 5, pp. 613–615, 2013.

[11] M. A. Tarasov, V. D. Gromov, G. D. Bogomolov, E. A. Otto, and L. S. Kuzmin, "Fabrication and characteristics of mesh band-pass filters," *Instrum. and Express Techn.*, vol. 52, no. 1, pp. 74–78, 2009.

[12] M. Tarasov, V. Edelman, S. Mahashabde, and L. Kuzmin, "Nonthermal optical response of superconductor-insulator-normal metal-insulator-superconductor tunnel structures," *JETPh*, vol. 119, no. 1, pp. 107–114, 2014.

[13] J. N. Ullom and P. A. Fisher, "Quasiparticle behavior in tunnel junction refrigerators," *Physica B*, vol. 284–288, pp. 2036–2038, 2000.

[14] G. O'Neil, "Improving NIS tunnel junction refrigerators: modelling, materials, and traps," Ph.D., Univ. Colorado, , 2011.

[15] M. Tarasov, V. Edelman, S. Mahashabde, and L. Kuzmin, "Power load and temperature dependence of cold-electron bolometer optical response at 350 GHz," *IEEE Trans. Appl. Supercond.*, vol. 24, no. 6, 2014, Art ID 2400105.

Mikhail A. Tarasov, photograph and biography not available at time of publication.

Valerian S. Edelman, photograph and biography not available at time of publication.

Andrey B. Ermakov, photograph and biography not available at time of publication.

Sumedh Mahashabde, photograph and biography not available at time of publication.

Leonid S. Kuzmin, photograph and biography not available at time of publication.